

Probing dark photons from a light scalar at Belle II

Kingman Cheung,^{a,b,c} Yongkyu Kim,^d Youngjoon Kwon,^d C.J. Ouseph,^{a,b} Abner Soffer,^e Zeren Simon Wang^{a,b}

^a*Department of Physics, National Tsing Hua University, Hsinchu 300, Taiwan*

^b*Center for Theory and Computation, National Tsing Hua University, Hsinchu 300, Taiwan*

^c*Division of Quantum Phases and Devices, School of Physics, Konkuk University, Seoul 143-701, Republic of Korea*

^d*Department of Physics, Yonsei University, Seoul 03722, Republic of Korea*

^e*School of Physics and Astronomy, Tel Aviv University, Tel Aviv 69978, Israel*

E-mail: cheung@phys.nthu.edu.tw, ykjk1401@yonsei.ac.kr,
yjkwon63@yonsei.ac.kr, ouseph444@gmail.com, asoffer@tau.ac.il,
wzs@mx.nthu.edu.tw

ABSTRACT: In the minimal $U(1)$ extension of the Standard Model (SM), a new gauge boson referred to as “dark photon” is predicted. The dark-photon mass can be generated from an additional Higgs mechanism associated with a dark scalar boson. At B -factories such as Belle II, large numbers of B -mesons are produced and can decay to a kaon plus the dark scalar via the latter’s mixing with the SM Higgs boson. We evaluate the sensitivity of Belle II for the case in which the dark scalar decays exclusively into a pair of dark photons via the new $U(1)$ gauge coupling, and the dark photons are long lived owing to a small kinetic mixing ϵ . We study the experimental signature in which each dark photon decays into a pair of charged leptons, pions, or kaons, resulting in a pair of displaced vertices, and argue that the search is essentially background-free. We perform detailed Monte-Carlo simulations to determine the expected number of signal events at Belle II with an integrated luminosity of 50 ab^{-1} , taking into account the efficiencies for both final-state-particle identification and displaced tracking. We find that for experimentally allowed values of the scalar mixing angle and kinematically allowed dark-photon and dark-scalar masses, the proposed search is uniquely sensitive to the medium- ϵ regime, which is currently mostly unexcluded by experiments.

Contents

1	Introduction	1
2	Model basics	3
3	Experiment and simulation	6
3.1	The Belle II experiment	6
3.2	Signal-candidate reconstruction	7
3.3	Potential background sources	8
3.4	Simulation procedure	10
4	Numerical results	14
5	Conclusions	16
A	Detector efficiencies for different final-state particles	17

1 Introduction

The existence of dark matter (DM) is strongly indicated by all astronomical observations, notably gravitational lensing, galactic rotation curves, the Bullet Cluster, and CMB measurements. Nevertheless, the nature and identity of the DM are entirely unknown. Most DM-particle searches have focused on a weakly interacting massive particle with mass $\mathcal{O}(10 - 1000)$ GeV (see for example Ref. [1]). Lack of a discovery in this scenario has expanded the interest to various DM-sector particles, defined as those that interact with the stable DM, and which may have mass of order GeV or even below. Typical examples of such particles include axions, axion-like particles, dark gauge bosons, dark scalars, and dark fermions [2–4].

Dark-sector models generically posit the existence of gauge bosons, scalar bosons, and fermions with a symmetry under which the Standard-Model (SM) particles are singlets. One of the simplest examples is a new gauge boson associated with a new $U(1)$ symmetry. Such a dark gauge boson, coined “dark photon” [5], can mix with the SM photon via a kinetic mixing term, $\epsilon F^{\mu\nu} F'_{\mu\nu}$, where $F_{\mu\nu}$ and $F'_{\mu\nu}$ denote the field strength of the SM photon and dark photon fields, respectively, and ϵ is the mixing coefficient. Kinetic mixing enables the dark photon mass eigenstate γ' to interact with SM particles, facilitating its creation and detection in experiments.

Various terrestrial experiments have established constraints on a dark photon with a mass $\gtrsim 1$ MeV. Signatures in which the dark-photon decay vertex is prompt or slightly displaced with respect to the beams interaction point (IP) were utilized in collider searches [6–12]. Signatures with highly displaced decays were studied at fixed-target and beam-dump

experiments [13–16]. In addition, bounds on energy losses in supernovae impose further limits in the region of small masses $m_{\gamma'} \lesssim \mathcal{O}(10^{-1})$ GeV. These limits were discussed in Refs. [17, 18] and updated in Refs. [19–21] to include the effect of finite temperature and plasma density as well as white dwarf bremsstrahlung. Also, the electron magnetic moment, with its very precise experimental determination, has been used to set an indirect limit [22]. For the mass range $m_{\gamma'} \sim 1$ MeV – 100 MeV, limits around $\epsilon \lesssim 10^{-10}$ have been determined from cosmology, arising from the cosmic microwave background and nucleosynthesis [23]. For a comprehensive list of the past experimental searches, we refer the reader to Refs. [24, 25]¹ and the references therein. Ref. [26] provides a summary of both current and prospective constraints on dark photons, as well as software for re-evaluating various dark-photon models.

In addition, a “dark scalar” or “dark-Higgs boson”, denoted ϕ_D , is naturally present in dark-sector models, particularly for generating the mass of the dark photon. The dark Higgs can couple to the SM Higgs doublet via a renormalizable term $\lambda(H^\dagger H)(\phi_D^\dagger \phi_D)$. These scalars are related through a mixing angle θ to the mass eigenstates ϕ and h_{125} , the latter being the scalar boson observed at the LHC. For the relation between λ and θ , see, for instance, Eq. (9) in Ref. [27]. The scalar mixing angle θ is constrained to be small by the LHC Higgs boson data [28], a number of fixed-target [29–40] and collider [41–43] experiments, as well as astrophysical observations of the supernovae SN1987a [44–47] and cooling in stars [20]. For a summary of these existing constraints, see Ref. [48].

Theoretical scenarios involving both the dark Higgs and the dark photon have been extensively studied from the collider-phenomenological and cosmological perspectives [5, 49–61], and signals have also been searched for at B factories [62–65]. Since the B -factory searches considered a different theoretical model from the one studied here, we find that their published bounds, both model-independent and model-dependent, cannot be reinterpreted as constraints on the model considered here. Therefore, we do not include them in the numerical results.

We note that the couplings of the dark Higgs² to the SM fermions and to the W - and Z -bosons are governed by the mixing angle θ , while the couplings of the dark photon to the SM fermions are dictated by ϵ . In addition, importantly, the dark Higgs couples to a pair of dark photons via the new gauge coupling associated with the appended $U(1)$ symmetry. This facilitates the decoupling of the production rate and the lifetime of the dark photon when it is produced in dark-scalar decays. In this paper we focus on the case in which $\phi \rightarrow \gamma'\gamma'$ is by far the dominant decay mode of the dark scalar, and the dark Higgs decays promptly.

Sensitive searches for a dark scalar and dark photon with masses around a GeV can be carried out at B -factories. For example, the Belle II experiment [66, 67] plans to produce as many as 5.5×10^{10} B -meson pairs in the coming decade. As a result, it can search for rare decays of the B -meson with branching ratios as small as $\mathcal{O}(10^{-10})$, as long as the

¹See also <https://cajohare.github.io/AxionLimits/docs/dp.html> for a graphical compilation of these existing limits.

²For clarification, we use the terms “dark Higgs/scalar” and “dark photon” to denote both the weak eigenstate and the mass eigenstate interchangeably, of the corresponding fields.

search channel has reasonably high efficiency and very low background.

In this work, we study the decay chain:

$$B^\pm \rightarrow K^\pm \phi, \quad \phi \rightarrow \gamma' \gamma',$$

followed by the displaced decay of each dark photon

$$\gamma' \rightarrow e^+ e^-, \mu^+ \mu^-, \pi^+ \pi^-, K^+ K^-.$$

This signal process was first proposed in Ref. [68] for study at B -factories (see also e.g. Refs. [69–73] for some recent phenomenological studies on Belle II sensitivities to long-lived dark photons). However, in this work we show how to improve the sensitivity to the kinetic mixing parameter ϵ down to $\mathcal{O}(10^{-7})$ for $m_\phi = 4$ GeV with $\theta = 10^{-4}$. The sensitivity reach varies mildly for m_ϕ in the range 0.1 – 4 GeV. An important factor leading to the high sensitivity is the focus on a region of parameter space in which the dark photons are long lived and their decays produce a pair of displaced vertices (DVs) in the detector. As we will show, our proposed search, compared to past experiments and other proposed searches, is sensitive to a unique parameter region in the medium- ϵ regime which is largely un-probed. Further, we emphasize that this is the first study of a search for dark photons at Belle II associated with a signature of double DVs consisting of two tracks each.

The organization of this paper is as follows. We lay out the basics of the model in Sec. 2. In Sec. 3, we introduce the Belle II experiment, discuss the signal-event reconstruction and background sources at the experimental level, and describe the signal-event simulation procedure. Sec. 4 contains our numerical results of the Belle II sensitivity reach in terms of the dark-photon and dark-Higgs parameters. We summarize the work in Sec. 5. Additionally, in Appendix A, we report the detector efficiencies that we estimate for the different final states.

2 Model basics

We explore an extension of the SM with an additional, dark-sector $U(1)_D$ gauge symmetry, under which all SM particles are neutral. The gauge boson associated with this symmetry is referred to as the dark photon and denoted γ' in this paper. The $U(1)_D$ symmetry undergoes spontaneous breaking through the vacuum expectation value (vev) of a complex scalar field ϕ_D , which carries a $U(1)_D$ charge. As a result, the dark photon gains mass $m_{\gamma'}$. Furthermore, an interaction term between two dark photons and the CP -even component of ϕ_D appears. The interaction strength is determined by $m_{\gamma'}$ and the $U(1)_D$ gauge coupling g' . Following the electroweak symmetry breaking, the dark photon can mix with the photon through the gauge kinetic mixing term between the SM hypercharge and the $U(1)_D$ gauge field. We label the coefficient of the kinetic-mixing term with ϵ . The dark photon can thus interact with the SM fermions through the electromagnetic current. Taking the scalar mixing angle θ to be small, the interaction Lagrangian is [60]

$$\mathcal{L}_{\text{int}} = g' m_{\gamma'} \phi \gamma'_\mu \gamma'^\mu - \epsilon e \gamma'_\mu J_{\text{EM}}^\mu + \sum_f \frac{m_f \theta}{v} \phi \bar{f} f, \quad (2.1)$$

where v is the SM Higgs vev, $e = \sqrt{4\pi\alpha_{\text{QED}}}$ is the electromagnetic coupling with α_{QED} being the fine-structure constant, J_{EM}^μ denotes the SM electromagnetic current, and f labels each SM fermion with mass m_f .

At B -factories, the scalar mass eigenstate ϕ is dominantly produced through mixing with the SM Higgs in penguin, $b \rightarrow s\phi$ decays of B -mesons. We consider only the experimentally favorable $B^+ \rightarrow K^+\phi$ decay (and the charge-conjugated channel). For the computation of this decay's width, we follow Ref. [34]:

$$\Gamma(B^+ \rightarrow K^+\phi) \simeq |g_{\phi sb}|^2 \left| \langle K^+ | \bar{s}_L b_R | B^+ \rangle \right|^2 \frac{\lambda_{B^+, K^+\phi}^{1/2}}{16\pi m_{B^+}}, \quad (2.2)$$

where

$$g_{\phi sb} = \frac{\theta m_b}{v} \frac{3\sqrt{2} G_F m_t^2 V_{ts}^* V_{tb}}{16\pi^2}, \quad (2.3)$$

$$\lambda_{x,yz} \equiv \frac{m_x^2 - (m_y - m_z)^2}{m_x^2} \frac{m_x^2 - (m_y + m_z)^2}{m_x^2}, \quad (2.4)$$

with $m_{b/t}$ denoting the bottom/top quark mass, G_F being the Fermi constant, and V_{ts} and V_{tb} being CKM matrix elements. The $B^+ \rightarrow K^+$ transition matrix element can be approximated as [74, 75]

$$\left| \langle K^+ | \bar{s}_L b_R | B^+ \rangle \right|^2 = \frac{1}{4} \frac{(m_{B^+}^2 - m_{K^+}^2)^2}{(m_b - m_s)^2} f_K^2, \quad (2.5)$$

with

$$f_K = \frac{0.33}{1 - q^2/37.5 \text{ GeV}^2}, \quad (2.6)$$

where $q^2 = m_\phi^2$ is the transferred momentum squared.

The partial decay widths of the dark Higgs into dark photons and charged leptons are [60].

$$\Gamma(\phi \rightarrow \gamma'\gamma') = \frac{g'^2 m_{\gamma'}^2}{8\pi m_\phi} \left(2 + \frac{m_\phi^4}{4m_{\gamma'}^4} \left(1 - \frac{2m_{\gamma'}^2}{m_\phi^2} \right)^2 \right) \beta_\phi(\gamma'), \quad (2.7)$$

$$\Gamma(\phi \rightarrow f\bar{f}) = N_c \frac{m_\phi}{8\pi} \left(\frac{m_f}{v} \right)^2 \theta^2 \left(1 - \frac{4m_f^2}{m_\phi^2} \right) \beta_\phi(f), \quad (2.8)$$

where $\beta_i(j) = \sqrt{1 - 4m_j^2/m_i^2}$ is the kinematic factor of the decay $i \rightarrow jj$, and $N_c = 1$ (3) for f being a charged lepton (quark). It is noteworthy that the ϕ decay widths into SM fermions are suppressed by the scalar mixing θ (see Sec. 1). Thus, ϕ dominantly decays into a pair of dark photons [60, 76]. In practice, we simply assume that the dark Higgs boson ϕ decays promptly into a pair of dark photons with a branching ratio of 100%. This is justified with the findings in, for instance, Ref. [60], which shows that for $m_\phi = 2 \text{ GeV}$ and $\theta = 10^{-4}$, even setting g' to be as small as 10^{-4} renders $\mathcal{B}(\phi \rightarrow \gamma'\gamma') \simeq 100\%$ across almost the whole kinematic range of $m_{\gamma'}$ (see also Ref. [61] for a relevant discussion).

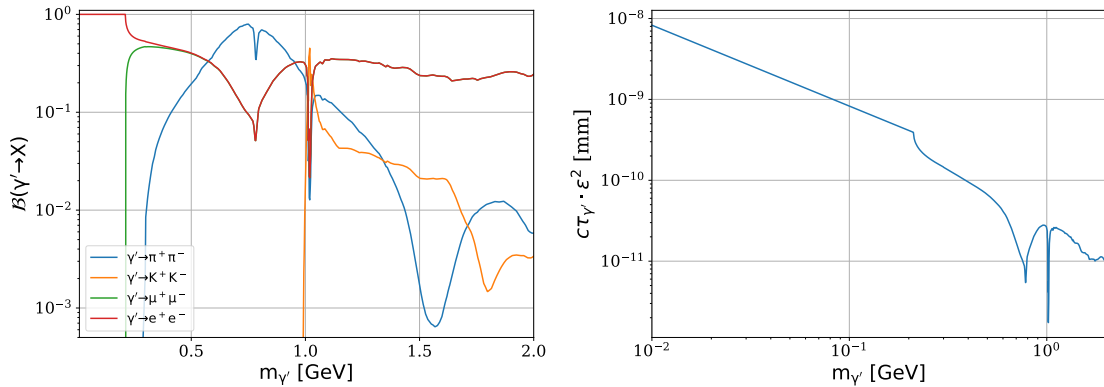


Figure 1. The dark-photon decay branching ratios into the signature final states (left), and its proper decay length re-scaled with the squared mixing coefficient ϵ^2 (right), as functions of the dark-photon mass. Note that in the left panel, the curves for electrons and muons overlap for $m_{\gamma'} \gtrsim 0.5$ GeV. The dip around 0.78 GeV is due to ρ and ω mesons. Wiggles visible mostly for $m_{\gamma'} > 1$ GeV arise from experimental fluctuations in the measurement of \mathcal{R}_h [79]. For discussion of further features on these curves, we refer to Ref. [26].

The partial decay widths of the dark photon into a pair of charged leptons or any hadronic state h (including the two-body states of interest $\pi^+\pi^-$ and K^+K^-) are [24, 52, 60, 77, 78]

$$\Gamma(\gamma' \rightarrow l^+l^-) = \frac{1}{3} \alpha_{\text{QED}} m_{\gamma'} \epsilon^2 \sqrt{1 - \frac{4m_l^2}{m_{\gamma'}^2}} \left(1 + \frac{2m_l^2}{m_{\gamma'}^2}\right), \quad (2.9)$$

$$\Gamma(\gamma' \rightarrow h) = \Gamma(\gamma' \rightarrow \mu^+\mu^-) \times \mathcal{R}_h(s = m_{\gamma'}^2), \quad (2.10)$$

where the cross-section ratio $\mathcal{R}_h(s) = \sigma_{e^+e^- \rightarrow h} / \sigma_{e^+e^- \rightarrow \mu^+\mu^-}$ is extracted from Ref. [26]. The total width of the dark photon, $\Gamma_{\gamma'}$, is the sum of Eq. (2.9) and Eq. (2.10), with h referring to all kinematically allowed hadronic states.

In the left panel of Fig. 1 we show the resulting branching fractions into the signature final states, e^+e^- , $\mu^+\mu^-$, $\pi^+\pi^-$, and K^+K^- , as functions of the dark-photon mass $m_{\gamma'}$. In addition, in the right panel of Fig. 1, we plot the $m_{\gamma'}$ dependence of $c\tau_{\gamma'} \cdot \epsilon^2$, the proper decay length of the dark photon normalized with respect to the squared mixing parameter. Here, $c\tau_{\gamma'} = \hbar c / \Gamma_{\gamma'}$, where c and \hbar label the speed of light and the reduced Planck constant, respectively.

We show in Fig. 2 the Feynman diagrams for the production and decay of the dark photons corresponding to the signature of interest.

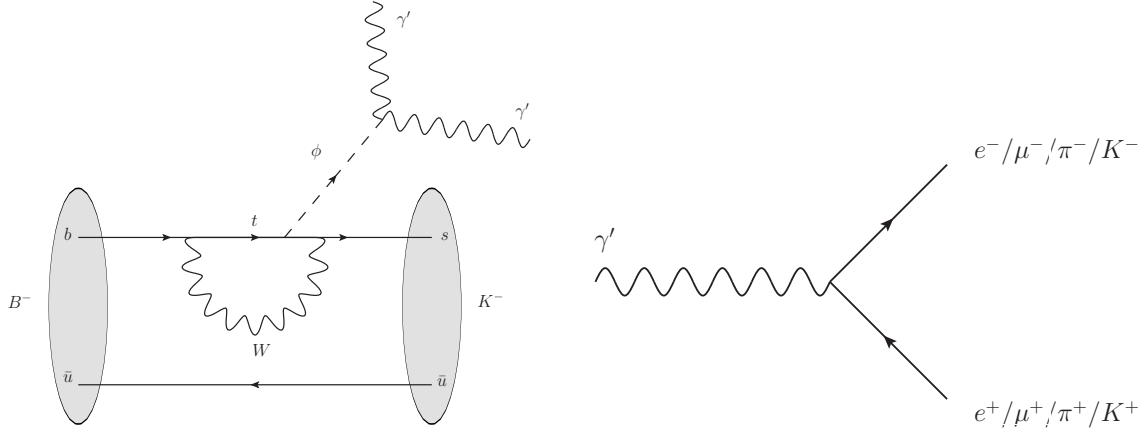


Figure 2. The Feynman diagrams for the production (left) and decay (right) of the long-lived dark photons at Belle II. For the production, a counterpart process for B^+ decays is implicitly included.

3 Experiment and simulation

3.1 The Belle II experiment

The Belle II experiment collects data at the SuperKEKB [80, 81] collider at KEK in Tsukuba, Japan. SuperKEKB collides electron and positron beams at 7 GeV and 4 GeV, respectively. The resulting center-of-mass (CM) energy corresponds to the mass of the $\Upsilon(4S)$ resonance, which decays promptly to two B -mesons. The Belle II detector [66, 67] is a magnetic spectrometer of a cylindrical structure placed around the beam IP, covering over 90% of the full 4π solid angle. The detector consists of several subdetectors. Closest to the interaction point are two layers of silicon-pixel detectors, surrounded by four layers of silicon strip detectors. These are used to track charged particles and measure decay-vertex positions with $\mathcal{O}(\mu\text{m})$ precision [82, 83]. Outside the vertex detectors is a helium-based small-cell drift chamber, which functions as the main tracking device and measures charged-particle momenta in 1.5 T magnetic field provided by a superconducting solenoid. Charged hadrons (e.g. π , K , and p) are identified mainly by endcap and barrel Cherenkov devices located outside the drift chamber, which are based on ring imaging and photon arrival times. Typical efficiencies for K and π identification are about 90%, while the rate for a π faking a K or vice versa is at the percent level [66, 84, 85]. Outside the Cherenkov devices, covering both barrel and endcap regions, is the electromagnetic calorimeter, which consists of 8736 CsI(Tl) crystals with a depth of about 16 radiation lengths. The calorimeter measures photon energies and provides electron identification with a typical efficiency of about 90% and a fake rate of under 1% in most kinematic range [86, 87]. Outside the superconducting coil that encloses the calorimeter is the muon and K_L^0 identification system, consisting of detectors placed between the magnetic flux return iron plates. The typical efficiency for muon identification is about 95%, with a fake rate of a few percent [86, 87].

3.2 Signal-candidate reconstruction

In what follows we describe the selection criteria that would likely be used in a future data analysis to suppress backgrounds and search for the signal. The kinematic region defined by these cuts is referred to as the signal region. As will be described below in Sec. 3.3, the background yield in the signal region is expected to be small. Consequently, the search method involves estimation of the expected background yield followed by determination of the statistical consistency of the observed signal-region yield with the background estimate. In case of consistency, one computes limits on the model parameter space. Conversely, an observed yield significantly larger than the expected background yield implies discovery of a signal and is followed by further studies of this signal.

Our signal process is $B^- \rightarrow K^- \phi$, with the dark scalar promptly undergoing the decay $\phi \rightarrow \gamma' \gamma'$. Each dark photon is reconstructed from its decay to two charged particles, which leave visible tracks in the detector and hence are denoted $t^+ t^-$. The $t^+ t^-$ final state is primarily $e^+ e^-$, $\mu^+ \mu^-$, and $\pi^+ \pi^-$, with a smaller $K^+ K^-$ contribution (see details in Fig. 1). We do not consider the decay $\gamma' \rightarrow p \bar{p}$, which is kinematically forbidden for almost all of the relevant $m_{\gamma'}$ range given the production mechanism considered here.

We focus on the case in which the dark photon is long lived, so that its decay position is visibly displaced from its production point, yet is inside the tracking volume of Belle II. Thus, the two tracks from each $\gamma' \rightarrow t^+ t^-$ decay form a DV. Requiring the two DVs to be significantly displaced from the interaction point of the collider beams strongly suppresses background from promptly produced tracks [88]. In our estimates (Sec. 3.4) we take the displacement requirement to be $r_{\text{DV}} > 1$ cm in the plane transverse to the collider beams, as in Ref. [89]. For consistency with the signal hypothesis and suppression of combinatorial, material-interaction, and K_L^0 -decay background (see Sec. 3.3), one will further require that the angle α between the $t^+ t^-$ momentum measured at the DV and the vector between the interaction point and the DV be small. For example, in Ref. [89] the requirement used was $\alpha < 0.01$. The $t^+ t^-$ invariant $m_{t^+ t^-}$ will be required to be large enough, e.g. $m_{t^+ t^-} > 20$ MeV, to suppress photon-conversion background. In addition, one will require the difference Δm between the invariant masses of the two dark-photon candidates to be smaller than 3 or 4 times its resolution $\sigma_{\Delta m}$. The typical invariant-mass resolution is a few MeV for r_{DV} of order centimeters from the interaction point (see, e.g. Fig. 6 of Ref [90] for the K_S^0 invariant-mass resolution in early Belle II data) and degrades slowly with increasing r_{DV} (see Chapter 9 of Ref. [91]).

Subsequently, standard selections used for B -meson reconstruction will be applied using the energy difference $\Delta E = E_B - \sqrt{s}/2$ and the beam-constrained mass $M_{bc} = \sqrt{s/4 - p_B^2}$. Here, E_B and p_B are the measured energy and momentum, respectively, of the B candidate in the CM frame of the $e^+ e^-$ collision, and s is the average squared CM energy of the collision. The value of s and the boost vector from the laboratory to the CM frame are known from calibration. Signal events are distributed as a peak around $\Delta E = 0$ and M_{bc} equal to the known mass of the B^+ meson [79]. The typical resolutions of these variables are $\sigma_{\Delta E} \approx 25$ MeV and $\sigma_{M_{bc}} \approx 2.5$ MeV for prompt decays, with slow degradation as a function of r_{DV} . We expect the cuts on ΔE and M_{bc} to be about 3 or 4

times their resolutions around the expected values for signal.

3.3 Potential background sources

We consider two general types of background: peaking background, which has a final-state signature that is similar to that of signal, and combinatorial background, which arises from random combinations of particles that meet the event-selection criteria by coincidence.

Peaking background arises from $B^+ \rightarrow K^+\pi^0$, $B^+ \rightarrow K^+\eta$, or $B^+ \rightarrow K^+\eta'$ with the π^0 , η , or η' decaying to two photons that undergo conversion to e^+e^- in detector material to form two DVs. In the case of the η , this background can be effectively suppressed by disregarding the $\gamma' \rightarrow e^+e^-$ channel when the scalar-candidate mass m_ϕ is close to $m_\eta \approx 0.5$ GeV. For $m_\phi \sim m_{\pi^0} \approx 0.135$ GeV, $\gamma' \rightarrow e^+e^-$ is the only kinematically allowed channel and must be used. This inevitably leads to reduced sensitivity for m_ϕ within about 10 MeV of m_{π^0} . We note that our sensitivity estimates are given for a sample of m_ϕ values that are far from the masses of the π^0 , η , and η' . Later in this subsection we discuss additional measures to suppress photon-conversion background from either peaking or combinatorial background.

The decay $B^+ \rightarrow K^+K_S^0K_S^0$ with $K_S^0 \rightarrow \pi^+\pi^-$ also constitutes peaking background for the $\gamma' \rightarrow \pi^+\pi^-$ signal mode. This background is suppressed very effectively by rejecting events in which $m_{t^+t^-}$ is close to the mass of the K_S^0 . In the other signal modes, this background contribution is very strongly suppressed by particle-identification criteria and, if needed, can be further suppressed by the above $m_{t^+t^-}$ cut, taking the track masses to be that of the pion. This approach was taken, e.g. in Ref. [89]. We note also that for $m_{\gamma'} \sim m_{K_S^0}$, the dark photon decays dominantly to lepton pairs, so the impact of the $\gamma' \rightarrow \pi^+\pi^-$ channel on the sensitivity is small and is not considered in our results.

After removing the peaking and the photon-conversions backgrounds, the dominant background is combinatorial. We estimate the abundance of this background in three steps. First, we consider the combinatorial background observed in BABAR and Belle analyses of related final states from prompt decays. Second, we consider the background-reduction impact of requiring DVs for the γ' decays. In the third step, we discuss the impact of having two γ' candidates in the signature.

In the first step, we consider the combinatorial background separately for leptonic and hadronic decays of the dark photons. For leptonic decays, one would like to use studies of B decays to a kaon and four leptons. However, lacking published results with this final state, we instead consider BABAR [92] and Belle [93] studies of $B^+ \rightarrow K^+\ell^+\ell^-$. Plots of M_{bc} for these studies exhibit 10-30 combinatorial-background events per ab^{-1} under the signal peak. Relative to $B^+ \rightarrow K^+\ell^+\ell^-$, our signal decay contains two additional leptons, yet softer particles overall. These differences, respectively, lead to a reduction and an increase in the expected background level, which we take to approximately cancel out. For hadronic final states, we estimate a background rate of about 500 events per ab^{-1} from the BABAR [94] study of $B^+ \rightarrow K^{*0}\pi^+\pi^-$. Since that study involved an 80-MeV-wide cut on the invariant mass of the $K^{*0} \rightarrow K^-\pi^+$ candidate, this estimate should be multiplied by roughly $\frac{1}{4}M_B/80 \text{ MeV} \approx 17$, where $\frac{1}{4}M_B$ is a rough estimate for the average invariant mass of two light particles in a 4-body decay. Thus, the resulting background level is

about 8500 events per ab^{-1} . For events in which one γ' decays leptonically and the other decays hadronically, one can expect the background to be the geometric average of the fully leptonic and fully hadronic final states, i.e. around 400 events per ab^{-1} .

In the second step, we note that the background level is greatly reduced by the requirement that the 4 displaced tracks originate from two DVs. For general discussions and examples of this background-suppression effect, see e.g. Refs. [88, 89, 95–97]. Background sources that give rise to a DV includes mostly true DVs from particle decays, with additional contributions from particle-material interactions and accidental spatial crossing of charged-particle tracks. We discuss these background sources in more detail in what follows.

True DVs are created in large numbers from the decays $K_S^0 \rightarrow \pi^+\pi^-$ and $\Lambda \rightarrow p\pi^-$. Such background is effectively rejected with m_{t+t^-} cuts, as discussed above. A smaller source of true-DV background is the decays $K_L^0 \rightarrow \pi^+\pi^-\pi^0$ and the $\mathcal{O}(\%)$ of $K_L^0 \rightarrow \pi^\pm\ell^\mp\nu$ decays that survive the particle-identification requirements. Given the long lifetime of the K_L , $c\tau_{K_L^0} \approx 15$ m, and its typical boost factor $\gamma_{K_L^0}\beta_{K_L^0} \sim 1$, only a few percent of K_L^0 mesons decay in the detector's tracking volume. Being three-body, these decays do not peak in the m_{t+t^-} mass, so they cannot be rejected by cutting on this variable. However, for the same reason, they are effectively suppressed by the α requirement (see Sec. 3.2).

DVs from particle-material interactions involve mainly photon conversions in the $\gamma' \rightarrow e^+e^-$ channel and hadronic interactions that mostly produce pions and eject protons or nuclear fragments. Accurate estimation of the contribution of material-interaction background to the final analysis requires full detector simulation with an event-sample size similar to that of the experimental sample, which would be beyond the scope of the current study. Therefore, we take aggressive measures to suppress the photon-conversion backgrounds, and briefly discuss the potential application of such methods to hadronic-interaction background as well. We note that following full-simulation study as part of the eventual experimental search, these requirements will be better tuned to the actual needs of the analysis.

Material-interaction background can be suppressed by vetoing DVs that are inside or near dense detector material layers. Mapping the material in sufficient detail is a technical challenge, which may be avoided altogether by requiring DVs to be inside the gaseous volume of the drift chamber. This approach was taken, e.g. in Ref. [96]. At Belle II, this corresponds to requiring the radial position of each DV to satisfy $r_{\text{DV}} > 16.8$ cm. In our study, we apply this requirement only in the e^+e^- channel for $m_{e^+e^-} < 100$ MeV, to suppress photon-conversion background. This requirement can be applied also for larger masses and other final states if this is determined needed by detailed detector simulation. It is important to note that the requirement $r_{\text{DV}} > 16.8$ cm leads to reduced sensitivity mostly at larger values of ϵ , which are probed with other methods, particularly prompt dark-photon decays. Material interactions occur also in the detector gas, but at a rate reduced by a factor of $\mathcal{O}(10^2)$ per DV. Nonetheless, to aggressively suppress photon-conversion background, we apply the cut $m_{e^+e^-} > 20$ MeV in the $\gamma' \rightarrow e^+e^-$ channel. Minimal requirements on m_{t+t^-} can also be considered for other channels following full detector simulation.

Displaced-vertex background may also arise from accidental spatial crossings of tracks.

Since the majority of tracks originate from close to the collider interaction point, this background is suppressed by requiring that the tracks forming the displaced vertex be inconsistent with originating from near the IP. Furthermore, for DVs that are outside the innermost detector layer, it is required that the tracks should not have detector hits at radii smaller than that of the DV.

In the third background-assessment step, we note that while the probability for occurrence of a single displaced vertex in background events is small, the probability for two such vertices is much smaller still. Additional background suppression arises from requiring the two γ' candidates to have consistent invariant masses (see e.g. Ref. [62]). Furthermore, the presence of two distinct vertices in the signal decay provides additional handles on background suppression if needed. For example, to further suppress photon-conversion background, one can allow only one of the two dark photons to decay via the di-electron channel. A similar criterion can be applied in the case of di-pion vertices to further suppress background from $K_S^0 \rightarrow \pi^+\pi^-$ with a badly mis-measured invariant mass and from $K_L^0 \rightarrow \pi^+\pi^-\pi^0$. Similarly, if the background for two hadronic DVs is determined to be too high in the final experimental analysis, these states can be discarded, requiring that at least one DV be leptonic. In our study we do not take such measures.

Starting from the initial background estimation of the first step and applying the background-suppression methods of the second and third steps, we conclude that the level of background can be reduced to the sub-event level without a large loss of signal efficiency, even with the full dataset of Belle II.

The above discussion is our a-priori estimation of the background. In the future data analysis, the expected number of background events will be more robustly estimated using a data-driven method. Generally, this involves counting the observed event yields in control regions designed to have negligible signal efficiency while containing many more background events than in the signal region. For example, requiring m_{t+t^-} to be around the K_S^0 mass or below about 20 MeV enhances the K_S^0 and photon-conversion background, respectively. A control region defined by, e.g. $10\sigma_{\Delta m} < \Delta m < 20\sigma_{\Delta m}$ can be used to enhance background from material-interaction, K_L^0 , and random-combination DVs. Another control region, defined by $10\sigma_{M_{bc}} < M_{bc} < 20\sigma_{M_{bc}}$, can be used to study all sources of background. From the observed event yields in the control regions one can estimate the background yields in the signal region using simulation. The procedure can be validated by using validation regions, defined similarly to the control regions but with different numerical values of the cuts, e.g. $5\sigma_{M_{bc}} < M_{bc} < 10\sigma_{M_{bc}}$.

3.4 Simulation procedure

In order to perform numerical simulation of the signal process described in Sec. 3.2, we employ the Monte-Carlo (MC) event generator MadGraph5aMC@NLO [98, 99] with the UFO model file HAHM³ [5, 55]. Since the model entails only flavor-diagonal interactions for the dark scalar ϕ , we introduce an effective vertex associated with the $b-s-\phi$ interaction and subsequently modify the UFO model file with FeynRules [100].

³The model file is available for download at <https://github.com/davidrcurtin/HAHM>.

At the operation level of the event generation we generate the process $e^+e^- \rightarrow b\bar{b}$. The electron and positron beams have energies of 7 and 4 GeV, respectively, corresponding to a CM energy of $\sqrt{s} = 10.58$ GeV. The bottom quark (b) then undergoes the decay $b \rightarrow s\phi$. The ϕ decays into a pair of dark photons. No parton-level cuts are applied. Our simulation is operated at the quark level, while the physical process is $e^+e^- \rightarrow B^+B^-$, with $B^+ \rightarrow K^+\phi$. Naively, this should lead to the simulation of wrong angular distributions. However, we set the b - and s -quarks masses to those of the B^+ - and K^+ mesons, respectively, so that the b quarks have very little velocity in the CM frame. This results in the s quarks and ϕ bosons being uniformly distributed in $\cos\theta_p^*$ (where θ_p^* is the polar angle with respect to the beams in the CM frame), as is the case in the physical process.

We perform parameter scans of the model in m_ϕ , $m_{\gamma'}$, and ϵ . We choose five representative values of m_ϕ ranging from 0.1 GeV to 4.0 GeV. For each value of m_ϕ , we simulate samples with different values of $m_{\gamma'}$ from 0.02 GeV to $m_\phi/2$. The MadGraph5 simulation outputs LHE files [101] containing the signal-event information. We apply the Python-based tool Pylhe [102] to read in these files and then perform further analysis and computation.

For each simulated sample, we use the kinematics of the simulated events to calculate the expected number of observed signal events at the Belle II experiment for different values of ϵ :

$$N_S(m_\phi, m_{\gamma'}, \epsilon) = 2 \times N_{e^+e^- \rightarrow B^+B^-} \times \mathcal{B}(B^+ \rightarrow K^+\phi) \times \mathcal{B}(\phi \rightarrow \gamma'\gamma') \times \epsilon^{\text{trk}} \times \sum_{t_{i,j}=e,\mu,\pi,K} \epsilon_{ij}^{\text{PID}} \cdot \mathcal{B}(\gamma' \rightarrow t_i^+t_i^-) \times \mathcal{B}(\gamma' \rightarrow t_j^+t_j^-), \quad (3.1)$$

where $N_{e^+e^- \rightarrow B^+B^-} = 2.75 \times 10^{10}$ is the predicted number of B^+B^- events at Belle II with an integrated luminosity of 50 ab^{-1} ; \mathcal{B} indicates a branching fraction⁴; ϵ^{trk} is the tracking efficiency, defined as the average probability of detecting both dark-photon decays in the event; and $\epsilon_{ij}^{\text{PID}}$ is the particle identification efficiency, defined as the probability to identifying the displaced tracks as electrons, muons, pions, or kaons according to the final state given by the indices i, j .

The tracking-related signal efficiency is calculated as:

$$\epsilon^{\text{trk}} = \frac{1}{N_{\text{sim}}} \sum_{k=1}^{N_{\text{sim}}} P^{\gamma'_{k1}} P^{\gamma'_{k2}}, \quad (3.2)$$

where N_{sim} is the total number of the simulated events and $P^{\gamma'_{k1}}$ and $P^{\gamma'_{k2}}$ represent, respectively, the probabilities of the first and the second dark photons in the k^{th} simulation event to be detected. For event k , the probability for detection of dark photon n is calculated as

$$P^{\gamma'_{kn}} = \frac{1}{R} \int_0^{80 \text{ cm}} L(r)A(z)e^{-\frac{r}{R}} dr, \quad (3.3)$$

where $R = (p_T^{\gamma'_{kn}}/m_{\gamma'})c\tau_{\gamma'}$ is the average transverse flight distance of the dark photon n before its decay, with $p_T^{\gamma'_{kn}}$ being its simulated transverse momentum, and the lifetime $\tau_{\gamma'}$

⁴Recall that we take $\mathcal{B}(\phi \rightarrow \gamma'\gamma') \simeq 1$; see Sec. 2

being determined from $m_{\gamma'}$ and ϵ (see Sec. 2); and $z = r \cot \theta_p$ is the longitudinal coordinate for the decay position of the dark photon that corresponds to the radial coordinate r , with θ_p being the polar angle of the dark photon in the laboratory frame. Furthermore, the function

$$A(z) = \begin{cases} 1, & -40 < z < 120 \text{ cm} \\ 0, & \text{otherwise} \end{cases} \quad (3.4)$$

represents the longitudinal extent $-40 < z < 120$ cm of the fiducial volume of the tracking volume, within which DVs can be detected. Lastly, the function

$$L(r) = \begin{cases} 1 - \frac{r}{80 \text{ cm}}, & 1 < r < 80 \text{ cm} \\ 0, & \text{otherwise} \end{cases} \quad (3.5)$$

corresponds to the radial extent $1 < r < 80$ cm of the fiducial volume, our cut $r_{\text{DV}} > 1$ cm⁵, and a linear drop in the tracking efficiency with radius. This approximate parameterization of the fiducial volume and tracking efficiency follows Refs. [96, 97, 103, 104].

We present in the upper panels of Fig. 3 density maps of ϵ^{trk} in terms of the kinetic mixing parameter ϵ and the dark-photon mass $m_{\gamma'}$, for two benchmark dark-Higgs masses $m_\phi = 1.0$ and 4.0 GeV. One observes that in large parts of the parameter space, ϵ^{trk} is of order 10%. We note that the blank space in these plots is where the computed value of ϵ^{trk} is below the machine precision and thus considered as zero.

The particle-identification efficiency $\epsilon_{ij}^{\text{PID}}$ is calculated with a separate simulation. We use the EVTGEN [105] event generator to produce the signal decays, employing the following models within EVTGEN. The decay $B^+ \rightarrow K^+\phi$ is produced with the PHSP phase-space model. The decay $\phi \rightarrow \gamma'\gamma'$ is generated with the SVV_HELAMP model, with either the longitudinal helicity amplitude H_0 being non-zero or the two transverse amplitudes H_\pm being non-zero and equal with a 0 relative phase. The decays of the dark photon to two leptons or two hadrons are produced with the VLL and VSS models, respectively. For each set of m_ϕ and $m_{\gamma'}$ values we produce a sample of 10^5 events. We determine the particle-identification efficiency for each charged particle in each event based on Figs. 25, 23, and 28 of Ref. [106]. For kaons and pions, we take the efficiency to be 90% if the particle is within the angular acceptance range drift-chamber, $17^\circ < \theta_p < 150^\circ$. For leptons, we simplify the θ_p - and momentum-dependence of the efficiency extracted from Ref. [106] and report the result in Tables 1 and 2 in Appendix A. The event-level efficiency is the product of the efficiencies for the five tracks. For each event sample, the total particle-identification efficiency $\epsilon_{ij}^{\text{PID}}$ is the average event-level efficiency of the sample.

This procedure does not account for impact of the dark-photon decay position on the particle-identification efficiency, and is hence imprecise. This simplification is necessary within the scope of this work, since particle-identification efficiencies for displaced particles are not publicly available at this time. Since the dedicated particle-identification detectors (the Cherenkov devices, the calorimeter, and the muon system) are all outside the drift chamber, one expects our procedure to somewhat underestimate $\epsilon_{ij}^{\text{PID}}$. This is because a

⁵For $m_{\gamma'} < 0.1$ GeV and γ' decays into e^+e^- , the radius cut is $16.8 < r_{\text{DV}} < 80$ cm, see Sec. 3.1.

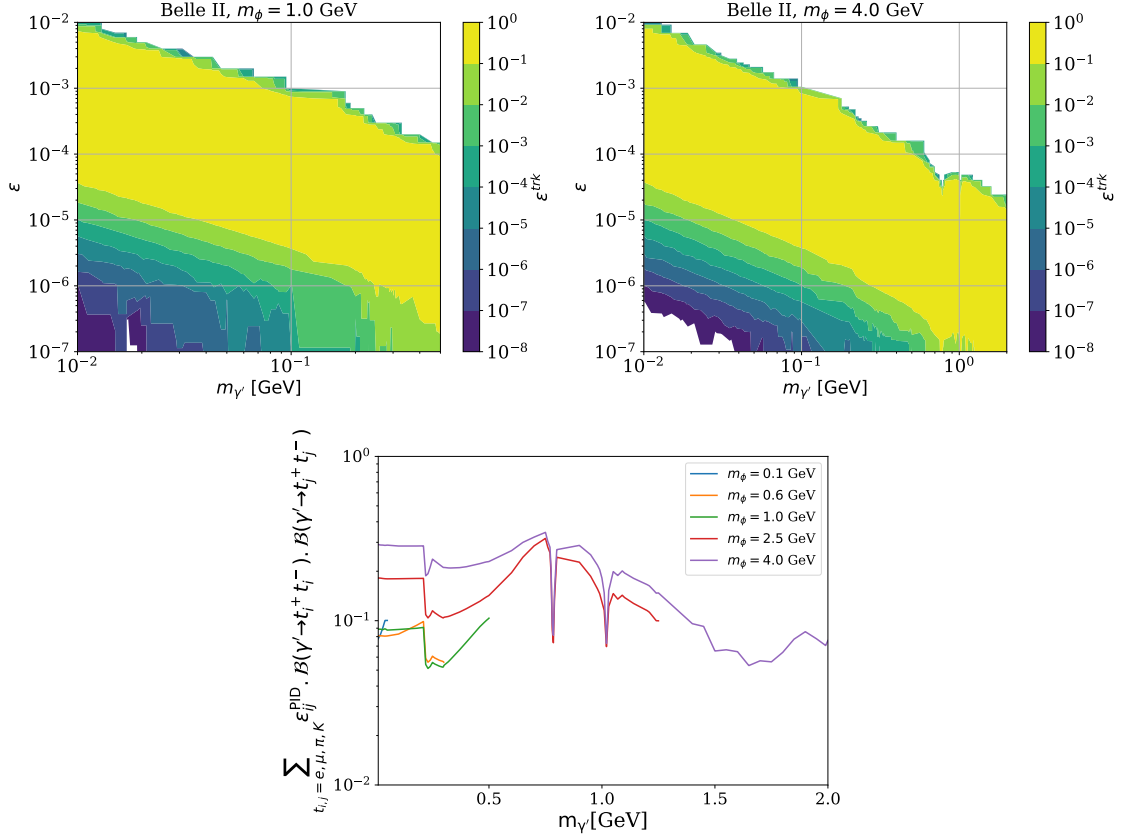


Figure 3. *Upper panels:* Density plot of ϵ^{trk} shown in the plane ϵ vs. $m_{\gamma'}$, for $m_\phi = 1.0$ GeV (*left*) and $m_\phi = 4.0$ GeV (*right*). The white-space parts are where ϵ^{trk} is so small that it is considered as zero by the machine. *Lower panel:* the sum of $\epsilon_{ij}^{\text{PID}} \cdot \mathcal{B}(\gamma' \rightarrow t_i^+ t_i^-) \cdot \mathcal{B}(\gamma' \rightarrow t_j^+ t_j^-)$ over all the dark-photon final-state combinations, as functions of $m_{\gamma'}$, for dark-Higgs masses of 0.1, 0.6, 1.0, 2.5, and 4.0 GeV.

charged particles produced at a DV is closer to the particle-identification detectors it is flying toward, and hence has a larger probability of hitting it.

In Figs. 5-14 of Appendix A we show the value of $\epsilon_{ij}^{\text{PID}}$ for each final state and for different values of m_ϕ and $m_{\gamma'}$.

Finally, in the lower panel of Fig. 3, we present the sum $\sum_{t_{i,j}=e,\mu,\pi,K} \epsilon_{ij}^{\text{PID}} \cdot \mathcal{B}(\gamma' \rightarrow t_i^+ t_i^-) \cdot \mathcal{B}(\gamma' \rightarrow t_j^+ t_j^-)$ (see Eq. (3.1)) as functions of the dark-photon mass $m_{\gamma'}$, for five representative dark-Higgs masses $m_\phi = 0.1, 0.6, 1.0, 2.5,$ and 4.0 GeV. Comparing this plot with Fig. 1, we conclude that the dominant factors in $\sum_{t_{i,j}=e,\mu,\pi,K} \epsilon_{ij}^{\text{PID}} \cdot \mathcal{B}(\gamma' \rightarrow t_i^+ t_i^-) \cdot \mathcal{B}(\gamma' \rightarrow t_j^+ t_j^-)$ are the branching ratios. Further, we note that the shapes of the curves shown in the lower plot of Fig. 3 will also help explain certain features of the sensitivity plots we will present in the next section.

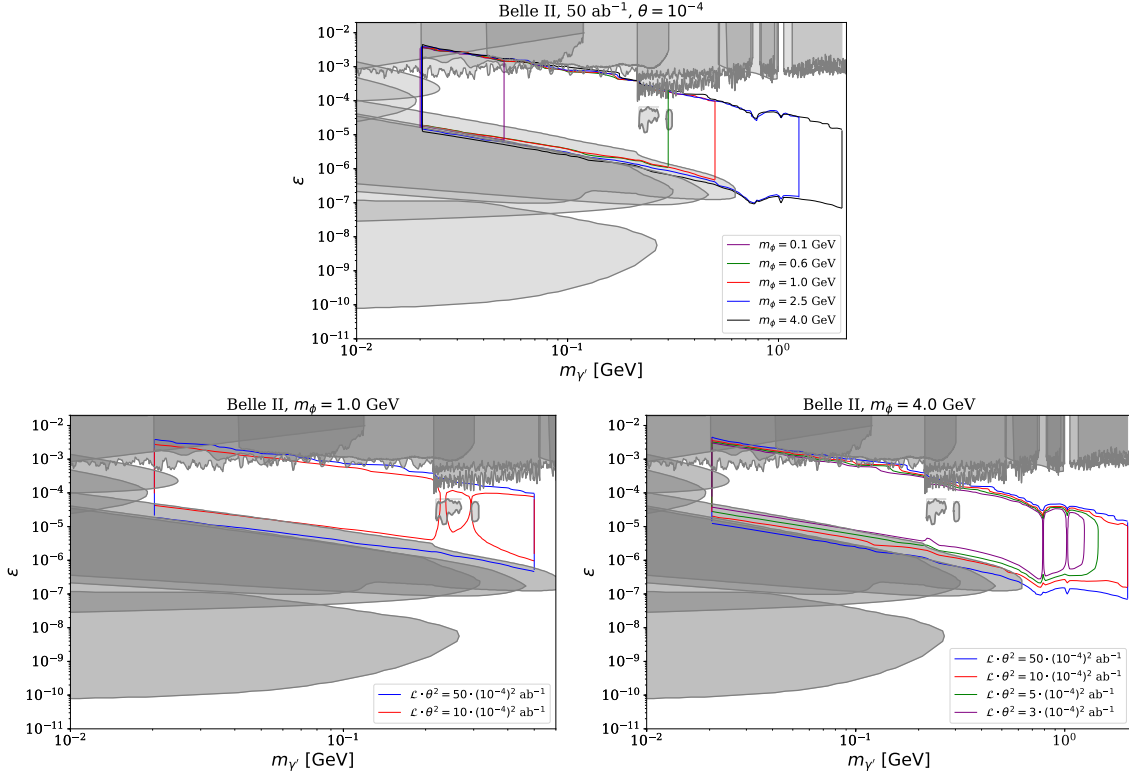


Figure 4. *Upper panel:* Sensitivity results for the case of fully longitudinal polarization shown in the plane ϵ vs. $m_{\gamma'}$, for various dark-Higgs masses with $\theta = 10^{-4}$. *Lower panels:* The same sensitivity results but for different choices of $\mathcal{L} \cdot \theta^2$, for $m_\phi = 1.0$ GeV (left) and 4.0 GeV (right). The gray areas represent the existing limits on the massive dark photon for $m_{\gamma'} \geq 10^{-2}$ GeV from di-lepton searches at collider/fixed target experiments (A1 [107], LHCb [108], BaBar [12], KLOE [109–112], and NA48/2 [16]), and previous beam dump experiments: E141 [13], E137 [113–115], ν -Cal [116, 117], and CHARM [118]. Bounds from supernovae [19] and $(g - 2)_e$ [22] are also shown together in gray.

4 Numerical results

We proceed to present numerical results in terms of the Belle II sensitivity for the signal.

Since the number of background events is expected to be smaller than 1 (see discussion in Sec. 3.3), we take the edge of the parameter-space region that is excluded at the 95% confidence level to be that for which observation of 3 signal events is expected based on Eq. (3.1). While we have calculated the particle-identification efficiency for both fully longitudinal and fully transverse polarizations, only the longitudinal-polarization case is used. The difference between the two cases is minor, and its magnitude can be gauged from the plots in Appendix A.

The results are shown in Fig. 4. In the upper panel, we overlap the sensitivity reach of Belle II with 50 ab^{-1} integrated luminosity for $m_\phi = 0.1, 0.6, 1.0, 2.5$ and 4.0 GeV. In this plot, the sensitivity results are presented in the $(m_{\gamma'}, \epsilon)$ plane for the scalar mixing angle

$\theta = 10^{-4}$, which is allowed by the existing bounds discussed in Sec. 1.

In the upper plot of Fig. 4, the region that can be excluded by Belle II with 50 ab^{-1} is the region enclosed by the curves. Along the top curve, the dark photon is short lived, so that not enough dark photons satisfy the minimal r_{DV} cut. Conversely, along the bottom curve the dark photon is long-lived. We note also that the lower dark-photon mass reach is due to the cut $m_{e^+e^-} > 0.02 \text{ GeV}$ used to suppress the photon-conversion background, and that the upper reach corresponds to the kinematic threshold $m_{\gamma'} < m_\phi/2$.

Comparing the different curves in the upper plot of Fig. 4, we observe that varying the dark-scalar mass does not have a significant impact on the sensitivity, except at the upper reach of the dark-photon mass determined by the kinematic threshold.

In the bottom plots, we consider $m_\phi = 1.0$ and 4.0 GeV , respectively, showing the Belle II's sensitivity reach in the plane ϵ vs. $m_{\gamma'}$, for different benchmarks of the combination $\mathcal{L} \cdot \theta^2$. With $m_\phi = 1.0 \text{ GeV}$, only for $\mathcal{L} \cdot \theta^2 = 50 \cdot (10^{-4})^2 \text{ ab}^{-1}$ and $10 \cdot (10^{-4})^2 \text{ ab}^{-1}$ more than 3 signal-events are predicted in certain regions of the parameter space, while with $m_\phi = 4.0 \text{ GeV}$ we find for all of $\mathcal{L} \cdot \theta^2 = (50, 10, 5, 3) \cdot (10^{-4})^2 \text{ ab}^{-1}$ Belle II can be sensitive to the model parameter space. This is mainly because the dependence of Eq. (2.6) on $q^2 = m_\phi^2$ rendering $\Gamma(B^+ \rightarrow K^+\phi)$ and hence the signal-event number grow with increasing m_ϕ . For values of $\mathcal{L} \cdot \theta^2$ lower than those shown, there is no sensitivity in both plots. Naively, in Fig. 4, we expect the lower sensitivity reach in ϵ to be proportional to $(\mathcal{L} \cdot \theta^2)^{-4}$, given vanishing background. This can be understood as follows. Along the lower curves in Fig. 4, the dark photon is expected to be in the large-decay-length regime where, roughly speaking, its boosted decay length is much larger than the distance from its production point to the outer edges of the fiducial volume; the tracking efficiency, and hence the signal-event rate N_S , are proportional to $\Gamma_{\gamma'}^2$, where the power of two arises from the required observation of two dark photons in each event. Since $\Gamma_{\gamma'} \propto \epsilon^2$ (see Eqs. (2.9), (2.10)), we conclude that $N_S \propto \epsilon^4$. Furthermore, $N_S \propto \mathcal{L} \cdot \theta^2$ (see Eqs. (2.2), (3.1)). As a result, decreasing $\mathcal{L} \cdot \theta^2$ by a factor of e.g. 10^4 leads to reduction in N_S by 10^4 , which can in turn be offset by increasing ϵ by 10. However, as we observe in e.g. the lower left plot of Fig. 4, lowering $\mathcal{L} \cdot \theta^2$ from 50 to 10 by a factor 5, the lower sensitivity reach in ϵ is weakened by more than $5^{1/4} \sim 1.5$; this arises from the fact that along the lower curves the dark photon is not long-lived enough to be in the large-decay-length limit.

We stress that the dark-photon production rate depends on θ^2 while its decay is mediated by the kinetic mixing parameter ϵ . This decoupling of the production and decay provides the advantage of expected large reach of our proposed search, compared to the minimal scenario where both the dark-photon production and decay are induced by ϵ .

Fig. 4 also shows as gray-shaded areas the current constraints on the dark-photon parameters, obtained from di-lepton searches conducted at colliders and fixed target experiments, including A1 [107], LHCb [108], BaBar [12], KLOE [109–112], and NA48/2 [16], the beam-dump experiments E141 [13], E137 [113–115], ν -Cal [116, 117], and CHARM [118], constraints from supernovae [19], and the electron anomalous magnetic moment [22].

The combination of the existing limits and our prediction for the Belle II sensitivity clearly demonstrates the importance of the Belle II search proposed here. Specifically, Fig. 4 shows that the medium- ϵ regime, which is currently mostly unexcluded, falls exactly

where Belle II is the most sensitive.

Finally, we explain some features observed in Fig. 4. For example, the lower left plot shows islands of the red curves separated at about 0.21 GeV and 0.28 GeV, which reflect the behavior of $\sum_{t_{i,j}=e,\mu,\pi,K} \varepsilon_{ij}^{\text{PID}} \cdot \mathcal{B}(\gamma' \rightarrow t_i^+ t_i^-) \cdot \mathcal{B}(\gamma' \rightarrow t_j^+ t_j^-)$ as shown in Fig. 3, corresponding to the dimuon and di-pion thresholds, respectively. Similarly, in the lower right panel the purple curves present also islands separated at around 0.8 and 1.0 GeV, which are due to not only the behavior of the curves displayed in Fig. 3 but also the sudden sharp increase of the dark-photon total decay width as plotted in the right panel of Fig. 1 arising from the ρ, ω , and ϕ resonances. We also comment that the zigzag in the upper curves in each plot is due to insufficient statistics for the prompt regime, where only a small proportion of the generated events, those with largely boosted dark photons, contribute significantly to the computation of N_S .

5 Conclusions

In this paper we propose a displaced-vertex-based search for long-lived dark photons at the ongoing experiment Belle II, in the theoretical framework of a hidden sector with a dark scalar. At Belle II, B^\pm mesons are pair-produced and can decay to a charged kaon K^\pm and a light dark scalar ϕ . We consider the case of ϕ decaying exclusively to a pair of dark photons. Via kinetic mixing, the dark photons subsequently decay leptonically or hadronically. We restrict the study to the experimentally favorable final states e^+e^- , $\mu^+\mu^-$, $\pi^+\pi^-$, and K^+K^- . We further require that both dark photons decay inside the Belle II detector's tracking volume.

We elaborate on potential background sources and argue for their insignificance. We perform Monte-Carlo simulations with MadGraph5 and compute the expected number of observed signal events for different values of the kinetic-mixing coefficient ϵ , the dark-photon mass $m_{\gamma'}$, the dark-scalar mass m_ϕ , and a currently allowed value $\theta = 10^{-4}$ for the mixing angle between the dark scalar and the Standard-Model Higgs. In this simulation, we implement the displaced-tracking efficiency as a linear function of the transverse distance of the dark-photon decay position from the interaction point. Furthermore, using the EVT-GEN event generator and published information, we incorporate the particle-identification efficiency and its dependence on the final-state particles and their kinematics.

We report the sensitivity reach of our proposed search in terms of the region in ϵ vs. $m_{\gamma'}$ that Belle II can exclude at 95% confidence level with an integrated luminosity of $\mathcal{L} = 50 \text{ ab}^{-1}$. Given the lack of background, this region is taken to be that for which at least three signal events would be observed. These bounds are calculated for five benchmark values of the m_ϕ . We note that reduced sensitivity is expected for m_ϕ within about 10 MeV of the π^0 mass of 135 MeV, due to background from $B^+ \rightarrow K^+\pi^0$, $\pi^0 \rightarrow \gamma\gamma$, with the photons undergoing conversion to e^+e^- in detector material. Further, additional sensitivity plots are shown for various values of $\mathcal{L} \cdot \theta^2$, for $m_\phi = 1.0$ and 4.0 GeV. Our results show that the search we propose uniquely probes a large, unexcluded region.

Acknowledgment

A. S. is supported by grants from Israel Science Foundation, United States-Israel Binational Science Fund, Tel Aviv University, and EU Horizon 2020. Yk. K. and Yj. K. are supported by the National Research Foundation of Korea grant NRF-2022R1A2C1003993. A. S. and Yj. K. acknowledge support from Tel Aviv-Yonsei Exchange Program. K.C. and C.J.O. are supported by MoST under Grant no. 110-2112-M-007-017-MY3.

A Detector efficiencies for different final-state particles

Table 1 shows the electron-identification efficiency, based on use of the calorimeter only, as a function of momentum and polar angle. The muon-identification efficiency is presented in Table 2. The final particle-identification efficiency $\varepsilon_{ij}^{\text{PID}}$ is shown in Figs. 5-14 for each final state and for different masses of the dark Higgs and the dark photon.

e^\pm efficiency	$p < 0.3$	$0.3 < p < 1.0$	$p > 1.0$
$\theta < 17^\circ$	0.00	0.00	0.00
$17^\circ < \theta < 31.4^\circ$	0.00	0.81	0.96
$31.4^\circ < \theta < 32.2^\circ$	0.00	0.68	0.81
$32.2^\circ < \theta < 128.7^\circ$	0.00	0.81	0.96
$128.7^\circ < \theta < 130.7^\circ$	0.00	0.68	0.81
$130.7^\circ < \theta < 150^\circ$	0.00	0.77	0.91
$150^\circ < \theta$	0.00	0.00	0.00

Table 1. Simplified electron-identification efficiency with respect to momentum and polar angle [106].

μ^\pm efficiency	$p < 0.6$	$0.6 < p < 1.5$	$p > 1.5$
$\theta < 17^\circ$	0.00	0.00	0.00
$17^\circ < \theta < 110^\circ$	0.00	0.81	0.96
$110^\circ < \theta < 130^\circ$	0.00	0.76	0.90
$130^\circ < \theta < 150^\circ$	0.00	0.81	0.96
$150^\circ < \theta$	0.00	0.00	0.00

Table 2. Simplified muon-identification efficiency with respect to momentum and polar angle [106].

References

- [1] M. Schumann, *Direct Detection of WIMP Dark Matter: Concepts and Status*, *J. Phys. G* **46** (2019), no. 10 103003, [[arXiv:1903.03026](#)].
- [2] J. Beacham et al., *Physics Beyond Colliders at CERN: Beyond the Standard Model Working Group Report*, *J. Phys. G* **47** (2020), no. 1 010501, [[arXiv:1901.09966](#)].
- [3] P. Agrawal et al., *Feebly-interacting particles: FIPs 2020 workshop report*, *Eur. Phys. J. C* **81** (2021), no. 11 1015, [[arXiv:2102.12143](#)].

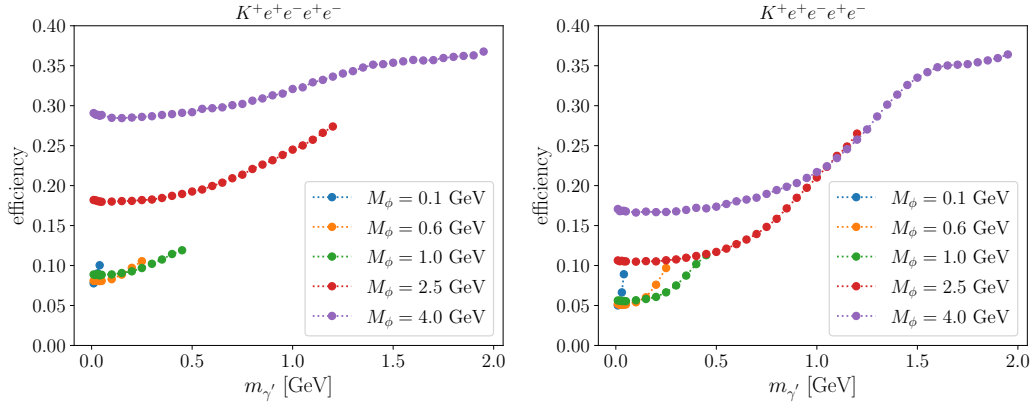


Figure 5. Estimated particle-identification efficiency of the $K^+e^+e^-e^+e^-$ final state with respect to the dark scalar mass and the dark-photon mass. The left figure shows results from fully longitudinal amplitude events and the right figure are for fully transverse amplitude events.

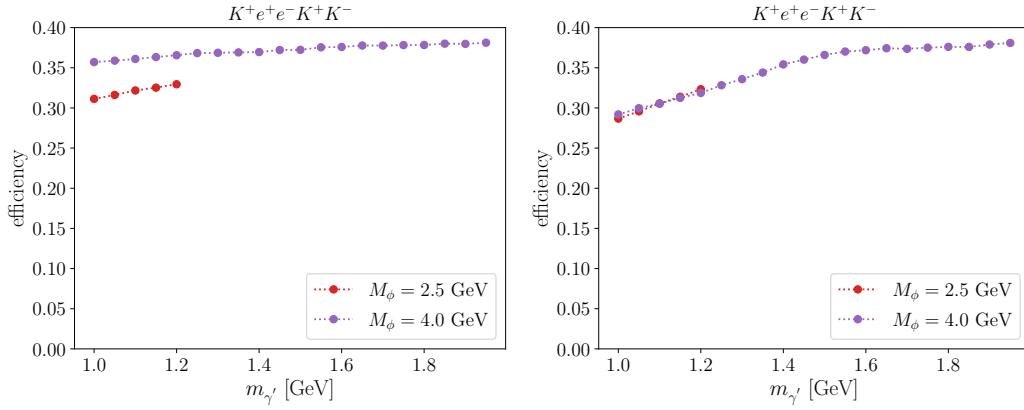


Figure 6. The same format as in Fig. 5 but for the $K^+e^+e^-K^+K^-$ final state.

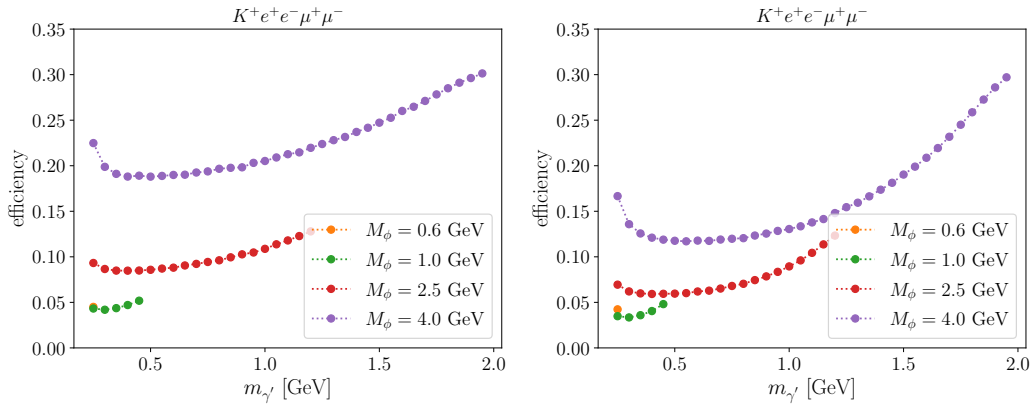


Figure 7. The same format as in Fig. 5 but for the $K^+e^+e^-\mu^+\mu^-$ final state.

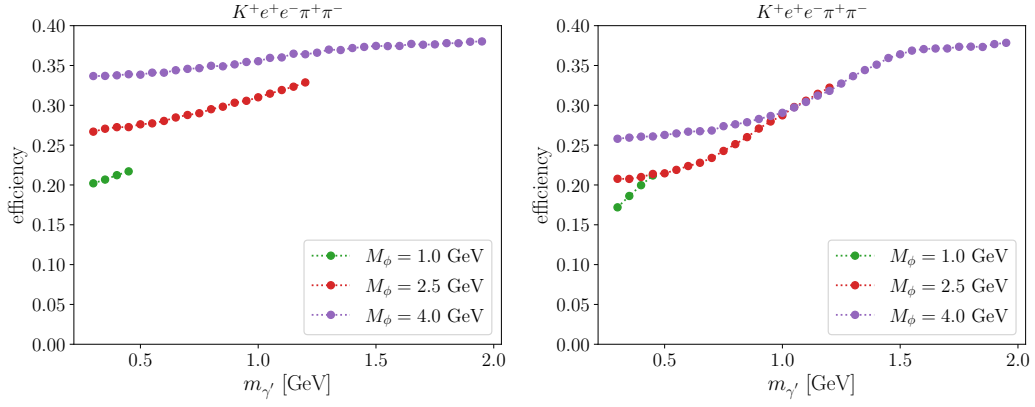


Figure 8. The same format as in Fig. 5 but for the $K^+e^+e^-\pi^+\pi^-$ final state.

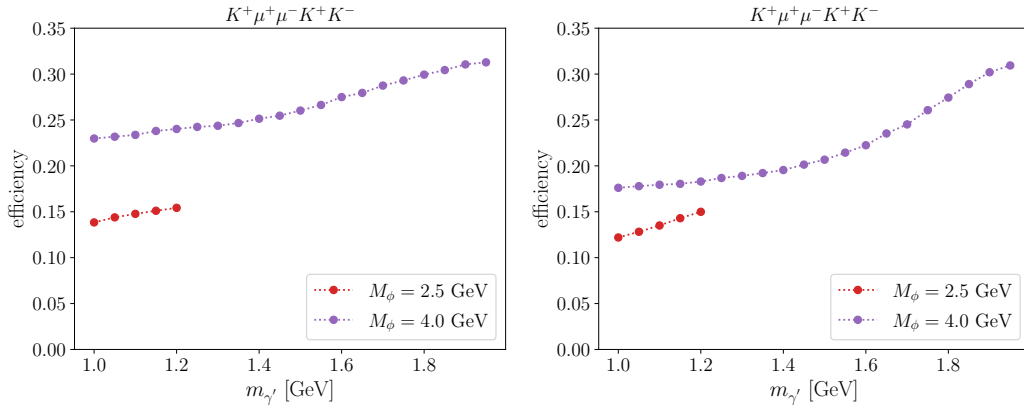


Figure 9. The same format as in Fig. 5 but for the $K^+\mu^+\mu^-K^+K^-$ final state.

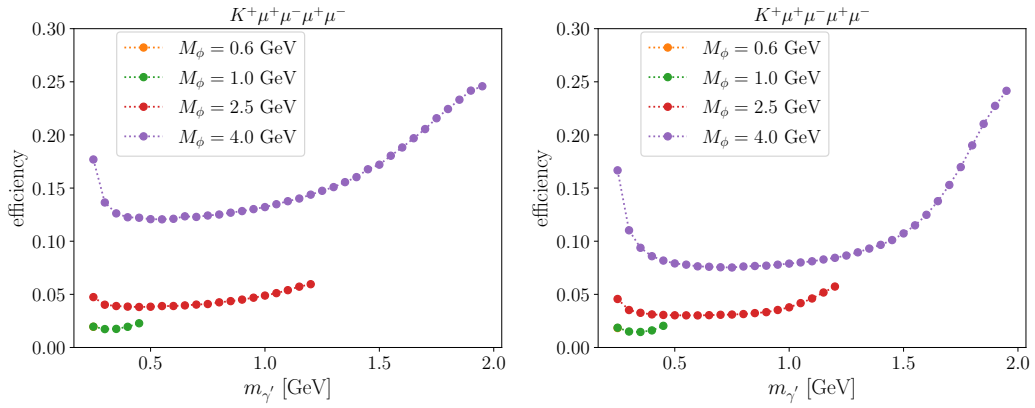


Figure 10. The same format as in Fig. 5 but for the $K^+\mu^+\mu^-\mu^+\mu^-$ final state.

(2023) 1122, [[arXiv:2305.01715](https://arxiv.org/abs/2305.01715)].

- [5] D. Curtin, R. Essig, S. Gori, and J. Shelton, *Illuminating Dark Photons with High-Energy Colliders*, *JHEP* **02** (2015) 157, [[arXiv:1412.0018](https://arxiv.org/abs/1412.0018)].

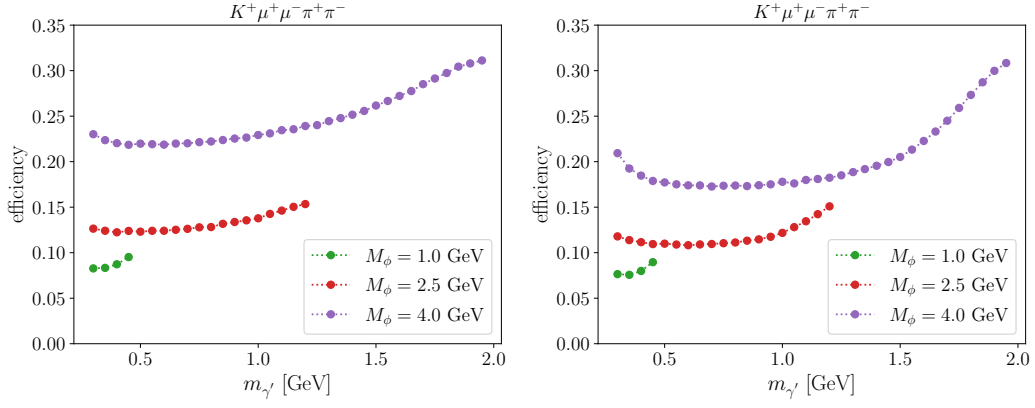


Figure 11. The same format as in Fig. 5 but for the $K^+\mu^+\mu^-\pi^+\pi^-$ final state.

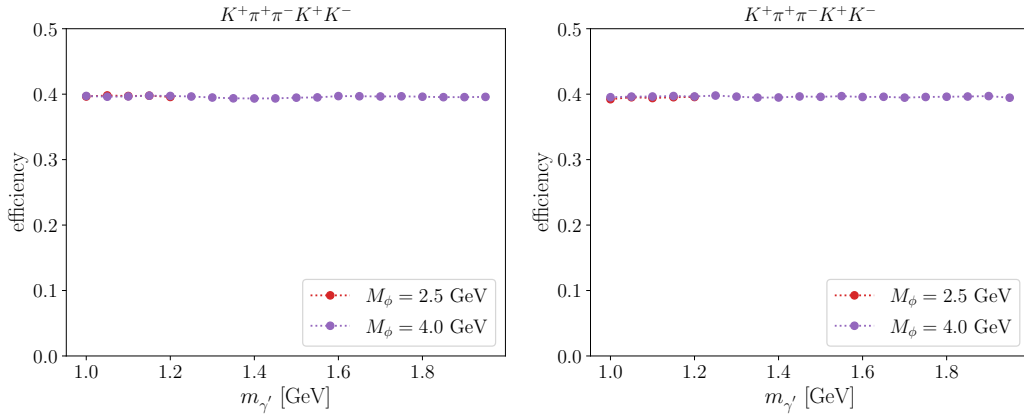


Figure 12. The same format as in Fig. 5 but for the $K^+\pi^+\pi^-K^+K^-$ final state.

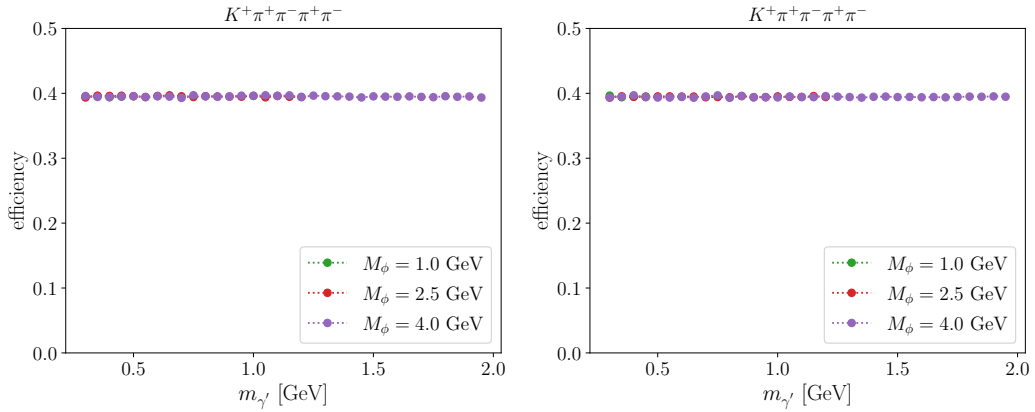


Figure 13. The same format as in Fig. 5 but for the $K^+\pi^+\pi^-\pi^+\pi^-$ final state.

[6] CMS Collaboration, *A search for pair production of new light bosons decaying into muons at $\sqrt{s}=13$ TeV*, .

[7] CMS Collaboration, *Search sensitivity for dark photons decaying to displaced muons with*

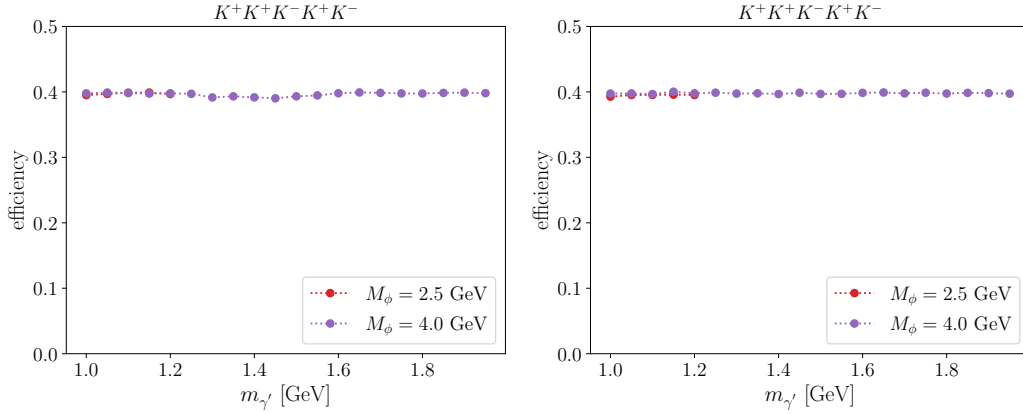


Figure 14. The same format as in Fig. 5 but for the $K^+K^+K^-K^+K^-$ final state.

CMS at the high-luminosity LHC, .

- [8] **ATLAS** Collaboration, G. Aad et al., *A search for prompt lepton-jets in pp collisions at $\sqrt{s} = 8$ TeV with the ATLAS detector*, *JHEP* **02** (2016) 062, [[arXiv:1511.05542](#)].
- [9] **ATLAS** Collaboration, G. Aad et al., *Search for long-lived neutral particles decaying into lepton jets in proton-proton collisions at $\sqrt{s} = 8$ TeV with the ATLAS detector*, *JHEP* **11** (2014) 088, [[arXiv:1409.0746](#)].
- [10] **ATLAS** Collaboration, *Search for long-lived neutral particles decaying into displaced lepton jets in proton-proton collisions at $\sqrt{s} = 13$ TeV with the ATLAS detector*, .
- [11] **LHCb** Collaboration, R. Aaij et al., *Search for Dark Photons Produced in 13 TeV pp Collisions*, *Phys. Rev. Lett.* **120** (2018), no. 6 061801, [[arXiv:1710.02867](#)].
- [12] **BaBar** Collaboration, J. P. Lees et al., *Search for a Dark Photon in e^+e^- Collisions at BaBar*, *Phys. Rev. Lett.* **113** (2014), no. 20 201801, [[arXiv:1406.2980](#)].
- [13] E. M. Riordan et al., *A Search for Short Lived Axions in an Electron Beam Dump Experiment*, *Phys. Rev. Lett.* **59** (1987) 755.
- [14] A. Bross, M. Crisler, S. H. Pordes, J. Volk, S. Errede, and J. Wrbanek, *A Search for Shortlived Particles Produced in an Electron Beam Dump*, *Phys. Rev. Lett.* **67** (1991) 2942–2945.
- [15] M. Davier and H. Nguyen Ngoc, *An Unambiguous Search for a Light Higgs Boson*, *Phys. Lett. B* **229** (1989) 150–155.
- [16] **NA48/2** Collaboration, J. R. Batley et al., *Search for the dark photon in π^0 decays*, *Phys. Lett. B* **746** (2015) 178–185, [[arXiv:1504.00607](#)].
- [17] J. B. Dent, F. Ferrer, and L. M. Krauss, *Constraints on Light Hidden Sector Gauge Bosons from Supernova Cooling*, [arXiv:1201.2683](#).
- [18] H. K. Dreiner, J.-F. Fortin, C. Hanhart, and L. Ubaldi, *Supernova constraints on MeV dark sectors from e^+e^- annihilations*, *Phys. Rev. D* **89** (2014), no. 10 105015, [[arXiv:1310.3826](#)].
- [19] J. H. Chang, R. Essig, and S. D. McDermott, *Revisiting Supernova 1987A Constraints on Dark Photons*, *JHEP* **01** (2017) 107, [[arXiv:1611.03864](#)].

- [20] E. Hardy and R. Lasenby, *Stellar cooling bounds on new light particles: plasma mixing effects*, *JHEP* **02** (2017) 033, [[arXiv:1611.05852](#)].
- [21] S. Bottaro, A. Caputo, G. Raffelt, and E. Vitagliano, *Stellar limits on scalars from electron-nucleus bremsstrahlung*, *JCAP* **07** (2023) 071, [[arXiv:2303.00778](#)].
- [22] M. Pospelov, *Secluded $U(1)$ below the weak scale*, *Phys. Rev. D* **80** (2009) 095002, [[arXiv:0811.1030](#)].
- [23] A. Fradette, M. Pospelov, J. Pradler, and A. Ritz, *Cosmological Constraints on Very Dark Photons*, *Phys. Rev. D* **90** (2014), no. 3 035022, [[arXiv:1407.0993](#)].
- [24] M. Bauer, P. Foldenauer, and J. Jaeckel, *Hunting All the Hidden Photons*, *JHEP* **07** (2018) 094, [[arXiv:1803.05466](#)].
- [25] A. Caputo, C. A. J. O’Hare, A. J. Millar, and E. Vitagliano, *Dark photon limits: a cookbook*, [arXiv:2105.04565](#).
- [26] P. Ilten, Y. Soreq, M. Williams, and W. Xue, *Serendipity in dark photon searches*, *JHEP* **06** (2018) 004, [[arXiv:1801.04847](#)].
- [27] K. Cheung and Z. S. Wang, *Probing Long-lived Particles at Higgs Factories*, *Phys. Rev. D* **101** (2020), no. 3 035003, [[arXiv:1911.08721](#)].
- [28] K. Cheung, P. Ko, J. S. Lee, and P.-Y. Tseng, *Bounds on Higgs-Portal models from the LHC Higgs data*, *JHEP* **10** (2015) 057, [[arXiv:1507.06158](#)].
- [29] S. Uemura, K. Liu, and M. X. Liu, *Direct search for dark photons with the seaquest spectrometer*, .
- [30] **CHARM** Collaboration, F. Bergsma et al., *Search for Axion Like Particle Production in 400-GeV Proton - Copper Interactions*, *Phys. Lett. B* **157** (1985) 458–462.
- [31] **NA62** Collaboration, E. Cortina Gil et al., *Search for π^0 decays to invisible particles*, *JHEP* **02** (2021) 201, [[arXiv:2010.07644](#)].
- [32] **NA62** Collaboration, E. Cortina Gil et al., *Measurement of the very rare $K^+ \rightarrow \pi^+ \nu \bar{\nu}$ decay*, *JHEP* **06** (2021) 093, [[arXiv:2103.15389](#)].
- [33] **BNL-E949** Collaboration, A. V. Artamonov et al., *Study of the decay $K^+ \rightarrow \pi^+ \nu \bar{\nu}$ in the momentum region $140 < P_\pi < 199$ MeV/c*, *Phys. Rev. D* **79** (2009) 092004, [[arXiv:0903.0030](#)].
- [34] M. W. Winkler, *Decay and detection of a light scalar boson mixing with the Higgs boson*, *Phys. Rev. D* **99** (2019), no. 1 015018, [[arXiv:1809.01876](#)].
- [35] **KTEV** Collaboration, A. Alavi-Harati et al., *Search for the Decay $K_L \rightarrow \pi^0 \mu^+ \mu^-$* , *Phys. Rev. Lett.* **84** (2000) 5279–5282, [[hep-ex/0001006](#)].
- [36] M. J. Dolan, F. Kahlhoefer, C. McCabe, and K. Schmidt-Hoberg, *A taste of dark matter: Flavour constraints on pseudoscalar mediators*, *JHEP* **03** (2015) 171, [[arXiv:1412.5174](#)]. [Erratum: *JHEP* 07, 103 (2015)].
- [37] D. Gorbunov, I. Krasnov, and S. Suvorov, *Constraints on light scalars from PS191 results*, *Phys. Lett. B* **820** (2021) 136524, [[arXiv:2105.11102](#)].
- [38] **KOTO** Collaboration, J. K. Ahn et al., *Study of the $K_L \rightarrow \pi^0 \nu \bar{\nu}$ Decay at the J-PARC KOTO Experiment*, *Phys. Rev. Lett.* **126** (2021), no. 12 121801, [[arXiv:2012.07571](#)].

- [39] D. Egana-Ugrinovic, S. Homiller, and P. Meade, *Light Scalars and the Koto Anomaly*, *Phys. Rev. Lett.* **124** (2020), no. 19 191801, [[arXiv:1911.10203](#)].
- [40] **MicroBooNE** Collaboration, P. Abratenko et al., *Search for a Higgs Portal Scalar Decaying to Electron-Positron Pairs in the MicroBooNE Detector*, *Phys. Rev. Lett.* **127** (2021), no. 15 151803, [[arXiv:2106.00568](#)].
- [41] **LHCb** Collaboration, R. Aaij et al., *Search for hidden-sector bosons in $B^0 \rightarrow K^{*0} \mu^+ \mu^-$ decays*, *Phys. Rev. Lett.* **115** (2015), no. 16 161802, [[arXiv:1508.04094](#)].
- [42] **LHCb** Collaboration, R. Aaij et al., *Search for long-lived scalar particles in $B^+ \rightarrow K^+ \chi(\mu^+ \mu^-)$ decays*, *Phys. Rev. D* **95** (2017), no. 7 071101, [[arXiv:1612.07818](#)].
- [43] **Belle-II** Collaboration, I. Adachi et al., *Search for a long-lived spin-0 mediator in $b \rightarrow s$ transitions at the Belle II experiment*, *Phys. Rev. D* **108** (2023), no. 11 L111104, [[arXiv:2306.02830](#)].
- [44] G. G. Raffelt, *Stars as laboratories for fundamental physics: The astrophysics of neutrinos, axions, and other weakly interacting particles*. 5, 1996.
- [45] G. Krnjaic, *Probing Light Thermal Dark-Matter With a Higgs Portal Mediator*, *Phys. Rev. D* **94** (2016), no. 7 073009, [[arXiv:1512.04119](#)].
- [46] **Kamiokande-II** Collaboration, K. Hirata et al., *Observation of a Neutrino Burst from the Supernova SN 1987a*, *Phys. Rev. Lett.* **58** (1987) 1490–1493.
- [47] P. S. B. Dev, R. N. Mohapatra, and Y. Zhang, *Revisiting supernova constraints on a light CP-even scalar*, *JCAP* **08** (2020) 003, [[arXiv:2005.00490](#)]. [Erratum: JCAP 11, E01 (2020)].
- [48] T. Ferber, A. Grohsjean, and F. Kahlhoefer, *Dark Higgs Bosons at Colliders*, [[arXiv:2305.16169](#)].
- [49] J. D. Wells, *How to Find a Hidden World at the Large Hadron Collider*, [[arXiv:0803.1243](#)].
- [50] M. Ahlers, J. Jaeckel, J. Redondo, and A. Ringwald, *Probing Hidden Sector Photons through the Higgs Window*, *Phys. Rev. D* **78** (2008) 075005, [[arXiv:0807.4143](#)].
- [51] S. Gopalakrishna, S. Jung, and J. D. Wells, *Higgs boson decays to four fermions through an abelian hidden sector*, *Phys. Rev. D* **78** (2008) 055002, [[arXiv:0801.3456](#)].
- [52] B. Batell, M. Pospelov, and A. Ritz, *Probing a Secluded $U(1)$ at B-factories*, *Phys. Rev. D* **79** (2009) 115008, [[arXiv:0903.0363](#)].
- [53] E. Weihs and J. Zurita, *Dark Higgs Models at the 7 TeV LHC*, *JHEP* **02** (2012) 041, [[arXiv:1110.5909](#)].
- [54] H. Davoudiasl, H.-S. Lee, I. Lewis, and W. J. Marciano, *Higgs Decays as a Window into the Dark Sector*, *Phys. Rev. D* **88** (2013), no. 1 015022, [[arXiv:1304.4935](#)].
- [55] D. Curtin et al., *Exotic decays of the 125 GeV Higgs boson*, *Phys. Rev. D* **90** (2014), no. 7 075004, [[arXiv:1312.4992](#)].
- [56] A. Falkowski and R. Vega-Morales, *Exotic Higgs decays in the golden channel*, *JHEP* **12** (2014) 037, [[arXiv:1405.1095](#)].
- [57] N. Bakhmet, M. Y. Khlopov, and T. Hussein, *Phenomenology of Hidden Abelian Higgs Model at Hadron Colliders using Neural Networks and Monte Carlo Techniques (Gauge Sector Z_{HAHM} & Scalar Sector H)*, [[arXiv:1507.02594](#)].

- [58] E. Izaguirre and D. Stolarski, *Searching for Higgs Decays to as Many as 8 Leptons*, *Phys. Rev. Lett.* **121** (2018), no. 22 221803, [[arXiv:1805.12136](#)].
- [59] K. Jodowski, F. Kling, L. Roszkowski, and S. Trojanowski, *Extending the reach of FASER, MATHUSLA, and SHiP towards smaller lifetimes using secondary particle production*, *Phys. Rev. D* **101** (2020), no. 9 095020, [[arXiv:1911.11346](#)].
- [60] T. Araki, K. Asai, H. Otono, T. Shimomura, and Y. Takubo, *Dark photon from light scalar boson decays at FASER*, *JHEP* **03** (2021) 072, [[arXiv:2008.12765](#)]. [Erratum: *JHEP* 06, 087 (2021)].
- [61] A. L. Foguel, G. M. Salla, and R. Z. Funchal, *(In)Visible signatures of the minimal dark abelian gauge sector*, *JHEP* **12** (2022) 063, [[arXiv:2209.03383](#)].
- [62] **BaBar** Collaboration, J. P. Lees et al., *Search for Low-Mass Dark-Sector Higgs Bosons*, *Phys. Rev. Lett.* **108** (2012) 211801, [[arXiv:1202.1313](#)].
- [63] **Belle** Collaboration, I. Jaegle, *Search for the dark photon and the dark Higgs boson at Belle*, *Phys. Rev. Lett.* **114** (2015), no. 21 211801, [[arXiv:1502.00084](#)].
- [64] **Belle** Collaboration, S. H. Park et al., *Search for the dark photon in $B^0 \rightarrow A'A'$, $A' \rightarrow e^+e^-$, $\mu^+\mu^-$, and $\pi^+\pi^-$ decays at Belle*, *JHEP* **04** (2021) 191, [[arXiv:2012.02538](#)].
- [65] **Belle-II** Collaboration, F. Abudinén et al., *Search for a Dark Photon and an Invisible Dark Higgs Boson in $\mu+\mu^-$ and Missing Energy Final States with the Belle II Experiment*, *Phys. Rev. Lett.* **130** (2023), no. 7 071804, [[arXiv:2207.00509](#)].
- [66] **Belle-II** Collaboration, T. Abe et al., *Belle II Technical Design Report*, [arXiv:1011.0352](#).
- [67] **Belle-II** Collaboration, W. Altmannshofer et al., *The Belle II Physics Book*, *PTEP* **2019** (2019), no. 12 123C01, [[arXiv:1808.10567](#)]. [Erratum: *PTEP* 2020, 029201 (2020)].
- [68] B. Batell, M. Pospelov, and A. Ritz, *Multi-lepton Signatures of a Hidden Sector in Rare B Decays*, *Phys. Rev. D* **83** (2011) 054005, [[arXiv:0911.4938](#)].
- [69] T. Ferber, C. Garcia-Cely, and K. Schmidt-Hoberg, *BelleII sensitivity to long-lived dark photons*, *Phys. Lett. B* **833** (2022) 137373, [[arXiv:2202.03452](#)].
- [70] T. Bandyopadhyay, *Dark Photons from displaced vertices*, [arXiv:2311.16997](#).
- [71] T. Bandyopadhyay, S. Chakraborty, and S. Trifinopoulos, *Displaced searches for light vector bosons at Belle II*, *JHEP* **05** (2022) 141, [[arXiv:2203.03280](#)].
- [72] B. Batell, N. Blinov, C. Hearty, and R. McGehee, *Exploring Dark Sector Portals with High Intensity Experiments*, in *Snowmass 2021*, 7, 2022. [arXiv:2207.06905](#).
- [73] J. Jaeckel and A. V. Phan, *Searching Dark Photons using displaced vertices at Belle II – with backgrounds*, [arXiv:2312.12522](#).
- [74] P. Ball and R. Zwicky, *New results on $B \rightarrow \pi, K, \eta$ decay formfactors from light-cone sum rules*, *Phys. Rev. D* **71** (2005) 014015, [[hep-ph/0406232](#)].
- [75] P. Ball and R. Zwicky, *$B_{d,s} \rightarrow \rho, \omega, K^*, \phi$ decay form-factors from light-cone sum rules revisited*, *Phys. Rev. D* **71** (2005) 014029, [[hep-ph/0412079](#)].
- [76] C.-F. Chang, E. Ma, and T.-C. Yuan, *Multilepton Higgs Decays through the Dark Portal*, *JHEP* **03** (2014) 054, [[arXiv:1308.6071](#)].
- [77] M. D’Onofrio, O. Fischer, and Z. S. Wang, *Searching for Dark Photons at the LHeC and FCC-he*, *Phys. Rev. D* **101** (2020), no. 1 015020, [[arXiv:1909.02312](#)].

- [78] M. Fabbrichesi, E. Gabrielli, and G. Lanfranchi, *The Dark Photon*, [arXiv:2005.01515](#).
- [79] **Particle Data Group** Collaboration, P. A. Zyla et al., *Review of Particle Physics*, *PTEP* **2020** (2020), no. 8 083C01.
- [80] Y. Ohnishi et al., *Accelerator design at SuperKEKB*, *PTEP* **2013** (2013) 03A011.
- [81] **SuperKEKB** Collaboration, K. Akai, K. Furukawa, and H. Koiso, *SuperKEKB Collider*, *Nucl. Instrum. Meth. A* **907** (2018) 188–199, [[arXiv:1809.01958](#)].
- [82] **Belle-II SVD** Collaboration, L. Zani et al., *The Silicon Vertex Detector of the Belle II experiment*, *Nucl. Instrum. Meth. A* **1038** (2022) 166952, [[arXiv:2206.11648](#)].
- [83] **Belle-II SVD** Collaboration, K. Adamczyk et al., *The design, construction, operation and performance of the Belle II silicon vertex detector*, *JINST* **17** (2022), no. 11 P11042, [[arXiv:2201.09824](#)].
- [84] **Belle-II** Collaboration, S. Sandilya, *Particle Identification at Belle II*, *J. Phys. Conf. Ser.* **770** (2016), no. 1 012045, [[arXiv:1610.00264](#)].
- [85] A. B. Kaliyar, *Particle Identification in Belle II Silicon Vertex Detector*, *Springer Proc. Phys.* **277** (2022) 763–767.
- [86] **Charged PID Group and Belle II** Collaboration, *Muon and electron identification efficiencies and hadron-lepton mis-identification rates at belle ii for moriond 2022*, .
- [87] M. Milesi, J. Tan, and P. Urquijo, *Lepton identification in Belle II using observables from the electromagnetic calorimeter and precision trackers*, *EPJ Web Conf.* **245** (2020) 06023.
- [88] L. Lee, C. Ohm, A. Soffer, and T.-T. Yu, *Collider Searches for Long-Lived Particles Beyond the Standard Model*, *Prog. Part. Nucl. Phys.* **106** (2019) 210–255, [[arXiv:1810.12602](#)]. [Erratum: *Prog.Part.Nucl.Phys.* 122, 103912 (2022)].
- [89] **BaBar** Collaboration, J. P. Lees et al., *Search for Long-Lived Particles in e^+e^- Collisions*, *Phys. Rev. Lett.* **114** (2015), no. 17 171801, [[arXiv:1502.02580](#)].
- [90] **Belle-II** Collaboration, S. Uno, *Commissioning and operation status of Belle II and SuperKEKB*, *PoS HQL2018* (2018) 072.
- [91] H. Kolanoski and N. Wermes, *Particle Detectors*. Oxford University Press, 6, 2020.
- [92] **BaBar** Collaboration, B. Aubert et al., *Direct CP, Lepton Flavor and Isospin Asymmetries in the Decays $B \rightarrow K^{(*)}\ell^+\ell^-$* , *Phys. Rev. Lett.* **102** (2009) 091803, [[arXiv:0807.4119](#)].
- [93] **BELLE** Collaboration, S. Choudhury et al., *Test of lepton flavor universality and search for lepton flavor violation in $B \rightarrow K\ell\ell$ decays*, *JHEP* **03** (2021) 105, [[arXiv:1908.01848](#)].
- [94] **BaBar** Collaboration, B. Aubert et al., *Branching fraction measurements of charged B decays to $K^{*+}K^+K^-$, $K^{*+}\pi^+K^-$, $K^{*+}K^+\pi^-$ and $K^{*+}\pi^+\pi^-$ final states*, *Phys. Rev. D* **74** (2006) 051104, [[hep-ex/0607113](#)].
- [95] **Belle** Collaboration, D. Liventsev et al., *Search for heavy neutrinos at Belle*, *Phys. Rev. D* **87** (2013), no. 7 071102, [[arXiv:1301.1105](#)]. [Erratum: *Phys.Rev.D* 95, 099903 (2017)].
- [96] C. O. Dib, J. C. Helo, M. Nayak, N. A. Neill, A. Soffer, and J. Zamora-Saa, *Searching for a sterile neutrino that mixes predominantly with ν_τ at B factories*, *Phys. Rev. D* **101** (2020), no. 9 093003, [[arXiv:1908.09719](#)].
- [97] S. Dey, C. O. Dib, J. Carlos Helo, M. Nayak, N. A. Neill, A. Soffer, and Z. S. Wang, *Long-lived light neutralinos at Belle II*, *JHEP* **02** (2021) 211, [[arXiv:2012.00438](#)].

- [98] J. Alwall, M. Herquet, F. Maltoni, O. Mattelaer, and T. Stelzer, *MadGraph 5 : Going Beyond*, *JHEP* **06** (2011) 128, [[arXiv:1106.0522](#)].
- [99] J. Alwall, R. Frederix, S. Frixione, V. Hirschi, F. Maltoni, O. Mattelaer, H. S. Shao, T. Stelzer, P. Torrielli, and M. Zaro, *The automated computation of tree-level and next-to-leading order differential cross sections, and their matching to parton shower simulations*, *JHEP* **07** (2014) 079, [[arXiv:1405.0301](#)].
- [100] A. Alloul, N. D. Christensen, C. Degrande, C. Duhr, and B. Fuks, *FeynRules 2.0 - A complete toolbox for tree-level phenomenology*, *Comput. Phys. Commun.* **185** (2014) 2250–2300, [[arXiv:1310.1921](#)].
- [101] J. Alwall et al., *A Standard format for Les Houches event files*, *Comput. Phys. Commun.* **176** (2007) 300–304, [[hep-ph/0609017](#)].
- [102] L. Heinrich, M. Feickert, and E. Rodrigues, “pylhe: v0.7.0.”
- [103] K. Cheung, A. Soffer, Z. S. Wang, and Y.-H. Wu, *Probing charged lepton flavor violation with axion-like particles at Belle II*, *JHEP* **11** (2021) 218, [[arXiv:2108.11094](#)].
- [104] E. Bertholet, S. Chakraborty, V. Loladze, T. Okui, A. Soffer, and K. Tobioka, *Heavy QCD axion at Belle II: Displaced and prompt signals*, *Phys. Rev. D* **105** (2022), no. 7 L071701, [[arXiv:2108.10331](#)].
- [105] D. J. Lange, *The EvtGen particle decay simulation package*, *Nucl. Instrum. Meth. A* **462** (2001) 152–155, [<https://evtgen.hepforge.org/doc/EvtGenGuide.pdf>].
- [106] **Belle-II** Collaboration, W. Altmannshofer et al., *The Belle II Physics Book*, *PTEP* **2019** (2019), no. 12 123C01, [[arXiv:1808.10567](#)]. [Erratum: *PTEP* 2020, 029201 (2020)].
- [107] H. Merkel et al., *Search at the Mainz Microtron for Light Massive Gauge Bosons Relevant for the Muon $g-2$ Anomaly*, *Phys. Rev. Lett.* **112** (2014), no. 22 221802, [[arXiv:1404.5502](#)].
- [108] **LHCb** Collaboration, R. Aaij et al., *Search for $A' \rightarrow \mu^+ \mu^-$ Decays*, *Phys. Rev. Lett.* **124** (2020), no. 4 041801, [[arXiv:1910.06926](#)].
- [109] **KLOE-2** Collaboration, F. Archilli et al., *Search for a vector gauge boson in ϕ meson decays with the KLOE detector*, *Phys. Lett. B* **706** (2012) 251–255, [[arXiv:1110.0411](#)].
- [110] **KLOE-2** Collaboration, D. Babusci et al., *Limit on the production of a light vector gauge boson in ϕ meson decays with the KLOE detector*, *Phys. Lett. B* **720** (2013) 111–115, [[arXiv:1210.3927](#)].
- [111] **KLOE-2** Collaboration, D. Babusci et al., *Search for light vector boson production in $e^+e^- \rightarrow \mu^+\mu^-\gamma$ interactions with the KLOE experiment*, *Phys. Lett. B* **736** (2014) 459–464, [[arXiv:1404.7772](#)].
- [112] **KLOE-2** Collaboration, A. Anastasi et al., *Limit on the production of a new vector boson in $e^+e^- \rightarrow U\gamma$, $U \rightarrow \pi^+\pi^-$ with the KLOE experiment*, *Phys. Lett. B* **757** (2016) 356–361, [[arXiv:1603.06086](#)].
- [113] J. D. Bjorken, S. Ecklund, W. R. Nelson, A. Abashian, C. Church, B. Lu, L. W. Mo, T. A. Nunamaker, and P. Rassmann, *Search for Neutral Metastable Penetrating Particles Produced in the SLAC Beam Dump*, *Phys. Rev. D* **38** (1988) 3375.
- [114] B. Batell, R. Essig, and Z. Surujon, *Strong Constraints on Sub-GeV Dark Sectors from SLAC Beam Dump E137*, *Phys. Rev. Lett.* **113** (2014), no. 17 171802, [[arXiv:1406.2698](#)].

- [115] L. Marsicano, M. Battaglieri, M. Bondi', C. D. R. Carvajal, A. Celentano, M. De Napoli, R. De Vita, E. Nardi, M. Raggi, and P. Valente, *Dark photon production through positron annihilation in beam-dump experiments*, *Phys. Rev. D* **98** (2018), no. 1 015031, [[arXiv:1802.03794](#)].
- [116] J. Blumlein and J. Brunner, *New Exclusion Limits for Dark Gauge Forces from Beam-Dump Data*, *Phys. Lett. B* **701** (2011) 155–159, [[arXiv:1104.2747](#)].
- [117] J. Blümlein and J. Brunner, *New Exclusion Limits on Dark Gauge Forces from Proton Bremsstrahlung in Beam-Dump Data*, *Phys. Lett. B* **731** (2014) 320–326, [[arXiv:1311.3870](#)].
- [118] S. N. Gninenko, *Constraints on sub-GeV hidden sector gauge bosons from a search for heavy neutrino decays*, *Phys. Lett. B* **713** (2012) 244–248, [[arXiv:1204.3583](#)].